RSC Advances

Check for updates

Adsorption of carbon dioxide by a novel amine impregnated ZSM-5/KIT-6 composite

Zhifeng Lin, [ID] Jianwen Wei, [ID]* Linlin Geng, Dejun Mei and Lei Liao

A novel amine modified composite was fabricated for CO_2 capture. Tetraethylenepentamine (TEPA) or polyethyleneimine (PEI) was selected to modify the micro/mesoporous ZSM-5/KIT-6 composite (ZK). With the porous nature of the support, large amine loadings from 50 to 80% were expected *via* a typical impregnation step. The CO_2 adsorption performance was investigated by thermal gravimetric analysis (TGA) in mixed gases (15% CO_2 and the balance is N_2) at 30–90 °C. With higher nitrogen content and better texture properties (surface area and total pore volume), TEPA-loaded materials exhibited better adsorption capacities than PEI-loaded materials. In the two series of samples, ZK-TEPA-60 and ZK-PEI-60 displayed outstanding CO_2 capture, with capacities as high as 5.32 and 4.59 mmol g^{-1} at 60 and 75 °C, respectively. ZK-TEPA-60 demonstrated relatively rapid kinetics and a higher enthalpy. The materials we designed displayed excellent CO_2 adsorption performance in comparison with other amine modified solid materials, indicating the prospects of these adsorbents for CO_2 capture from flue gas.

1. Introduction

The continuous increase in emissions of CO_2 mainly derived from burning a great deal of fossil fuels is aggravating climate change and global warming.[1,2] The reduction of CO_2 emissions is imperative for the mitigation of global warming for which capture of CO_2 from flue gas is an effective method. Recently, many kinds of CO_2 capture technologies have been developed to reduce CO_2 emissions.[3,4] Chemical absorption with amines has been commercialized on a large scale,[5–7] but there are many adverse effects, such as wastage of solvent due to amine volatilization, demand of high energy and generation of waste during regeneration and limitation of operational lifetime due to solvent degradation.[8–10] However, adsorption with porous solids has advantages, such as friendliness to the environment and long operational lifetime.[5,11] Therefore, there have been various porous materials designed as adsorbents for use in CO_2 capture, such as zeolites,[12,13] mesoporous silicas,[14,15] metal organic frameworks,[16–18] and activated carbons.[19,20]

Zeolites, a class of crystals with regular hole wall, such as ZSM-5, 13X, β, and 5A, have been widely used in industrial applications due to their excellent adsorption capacities at low CO_2 partial pressure and high reusability in regeneration. With medium pore size and abundant microporous structure, zeolite ZSM-5 is efficient for CO_2 capture through physisorption formed by van der Waals' force or hydrogen bonding. Hefti *et al.* found that the CO_2 uptake of ZSM-5 was 1.35 mmol g^{-1} at 25 °C and CO_2 partial pressure of 100 kPa and a higher value of

Guangxi Scientific Experiment Center of Mining, Metallurgy and Environment, Guilin University of Technology, Guilin 541004, PR China. E-mail: jianwen988@126.com

2.34 mmol g^{-1} was obtained as increasing pressure to 1000 kPa.[21] Mesoporous silicas, a class of silica-based inorganic materials with amorphous pore wall, such as KIT-6, SBA-15, MCM-48 and MCM-41, have been widely investigated due to high pore volume and surface area. With abundant mesoporous structure and large pore size, silica-based KIT-6 is beneficial to accommodate more amines to react with CO_2 for chemisorption. As a result, KIT-6 has demonstrated a better CO_2 adsorption performance over many other silica-based materials after impregnation with polyethyleneimine (PEI) as previously reported by Son *et al.*[22] At 75 °C and CO_2 partial pressure of 101 kPa, an maximum uptake of 3.07 mmol g^{-1} was found for PEI-loaded KIT-6.[22] The composites combined with zeolites and mesoporous silicas have common advantages, which are the optional adsorbents. Santos *et al.* fabricated micro/mesoporous composites containing zeolite ZSM-12 and mesoporous silica MCM-41 *via* the self-assembly procedure.[23] At 25 °C and CO_2 partial pressure of 101 kPa, the composite ZSM-12/MCM-41 displayed a better capacity (0.94 mmol g^{-1}) than those of ZSM-12 (0.86 mmol g^{-1}) and MCM-41 (0.27 mmol g^{-1}),[23] which is attributed to the synergistic effect. What's more, further improvement in the adsorption performance may be achieved after amine modification.

Inserting alkaline amine groups into adsorbents can improve CO_2 chemisorption, which can be normally achieved in three routes: amines anchored to the supports in the form of covalent bonds,[24,25] amines impregnated into the inner channel of supports[26,27] and amine containing polymers introduced directly without second modification by molecular imprinting technology.[28,29] In the first route, the grafted amines are usually aminosilanes. For instance, (3-aminopropyl) triethoxysilane

(APTES) was well grafted onto the surface of KIT-6 in dry solution, presenting a uptake of 0.9 mmol g^{-1} at CO_2 partial pressure of 100 kPa and 30 °C as reported by Kishor et al.[30] In the second route, PEI and tetraethylenepentamine (TEPA) are the usual modifying reagents. For example, PEI was impregnated into the inner channel of composite 5A@mesoporous silica fabricated via the sol–gel coating procedure as reported by Liu et al.[31] Besides, the amine containing polymers can also be used as grafted or impregnated amines. For example, the silica gel was grafted or impregnated with acrylamide polymer as reported by Zhao et al.[32] In the last route, the molecularly imprinted CO_2 adsorbents were developed by Zhao et al., using ethanedioic acid as template, acrylamide as functional monomer and ethylene glycol dimethacrylate as cross-linker.[28,29] Inspired by these reports, the composite support with amine loading would be a feasible strategy for designing amine modified solid composite.

Up to now, amine modified composites for CO_2 capture are rarely reported. Herein, an amine impregnated composite strategy was used to fabricate the two series of adsorbents, TEPA-loaded ZSM-5/KIT-6 and PEI-loaded ZSM-5/KIT-6. At the same time, it was found that there are many superiorities in amine impregnated ZSM-5/KIT-6 over the conventional silica-based materials, including high amine loading, high CO_2 adsorption capacity, high amine efficiency, rapid kinetics, high enthalpy and high regeneration performance.

2. Experimental

2.1. Preparation of support and amine loaded samples

ZSM-5/KIT-6 (Si/Al = 50) with molar composition of 1 TEOS:0.02 Al:0.017 P123:1.31 BuOH:195 H_2O:1.83 HCl was prepared through an assembly procedure.[33] First, 8.5 g of tetraethyl orthosilicate (TEOS, 99 wt%, Aldrich) was gradually dropped into the mixture of 16.87 g of distilled water, 4.54 g of tetrapropylammonium hydroxide solution (TPAOH, 25 wt%, Acros Organics) and 0.167 g of aluminium isopropoxide (AIP, 99.99 wt%, Acros Organics) with vigorous stirring at 35 °C for 2 h. Then, hydrothermal treatment was performed at 150 °C for 10 h, giving resultant sample ZSM-5 S_1. Second, 4 g of n-butanol

(BuOH, 99.5 wt%, Sinopharm Chem. Reagent Co.) was added into P123 solution containing 4 g of P123 ($EO_{20}PO_{70}EO_{20}$, M_w = 5800, Aldrich), 125 g of distilled water and 7.5 g of HCl (36 wt%, Xilong Chem. Reagent Co.). The mixture was stirred at 35 °C for 1 h, giving it S_2. Third, as cooling to room temperature, S_1 was uniformly added to S_2, and then stirred at 35 °C for 24 h before the hydrothermal process was performed at 100 °C for 24 h. As cooling to room temperature, the product was filtered, dried at 100 °C for 24 h and calcined at 550 °C for 6 h with a heating rate of 5 °C min^{-1}. The as-synthesized composite is denoted as ZK. The mass of precursor solution accounted for 18% of the mixture. The characterization methods for ZK, such as X-ray diffraction (XRD), nitrogen adsorption/desorption and scanning electron microscopy (SEM) can be seen in our previous study.[34]

TEPA or PEI was introduced into the ZK support by wet impregnation. The typical impregnation step carried out at atmospheric pressure was depicted as follows. A certain amount of TEPA or PEI was dispersed in 25 ml ethanol (Xilong Chem. Reagent Co.) under stirring for 30 min at room temperature. Subsequently, 0.5 g of ZK support was added under further stirring for 6.5 h. The ethanol was evaporated and the mixture was dried at 80 °C in air for 16 h. The samples are referred to ZK-TEPA-X or ZK-PEI-X (X = 50, 60, 70 or 80), where X stands for mass fraction of TEPA or PEI. For instance, ZK-TEPA-60 indicates that the ZK is loaded with 60% TEPA.

A schematic representation of the process for the preparation of ZK-PEI-X or ZK-TEPA-X is shown in Fig. 1.

2.2. Characterization

Thermal gravimetric and derivative thermogravimetric analysis (TGA/DTG) was performed on a SDT Q600 TGA (TA, USA) in nitrogen flow up to 800 °C.

Elemental analysis was carried out with a EA 2400 II elemental analyzer (Perkin-Elmer, USA) for nitrogen content of various samples.

Fourier transform infrared spectra (FTIR) were detected with a Nexus 470 IR spectrometer (Nicolet, USA) in wavenumber range of 4000–400 cm^{-1}. Detected wafers were made by mixing the samples and KBr with a mass ratio of 1 : 100.

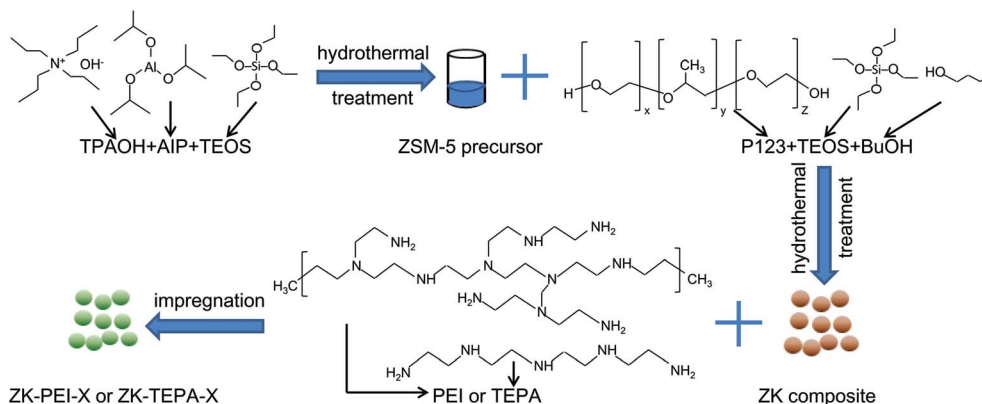

Fig. 1 Schematic representation of the preparation of ZK-PEI-X or ZK-TEPA-X.

Nitrogen adsorption/desorption tests were carried out at −196 °C with a NOVA2000e automatic surface analyzer (Quantachrome, USA). Each sample was outgassed at 100 °C in nitrogen atmosphere for 8 h before test. The surface area was calculated by Brunauer–Emmett–Teller (BET). Total pore volume was calculated from N_2 adsorption capacity at $P/P_0 = 0.99$.

2.3. CO$_2$ adsorption

CO$_2$ adsorption capacity was determined by SDT Q600 TGA (TA, USA) with a scale of 0.1 μg. In a typical experiment, a certain amount of sample was put in a 0.05 cm^3 platinum pan and regenerated (heated up to 110 °C with a heating rate of 10 °C min^{-1} and kept at 110 °C to get a constant weight) in N$_2$ (100 cm^3 min^{-1}) prior to adsorption. Then the sample was cooled to 60 °C before exposure to the CO$_2$/N$_2$ mixed gases (15 vol% CO$_2$) until the quantity of sample displayed no noticeable changes. The weight change and heat flow of amine modified ZK *versus* time were recorded. The adsorption capacity was calculated according to the following equation (eqn (1)) and enthalpy was calculated from the heat flow *versus* time and dry mass of sample according to the following equation (eqn (2)):

$$q_e = \frac{(m_e - m_d)/44.01}{m_d/1000} \tag{1}$$

$$H_{ads} = \frac{44.01 \varphi t}{1000 m_d} \tag{2}$$

where q_e is the equilibrium adsorption capacity of CO$_2$ (mmol g^{-1}), m_e and m_d are the sample weights after equilibrium and dehydration (mg), respectively, H_{ads} is the enthalpy (kJ mol^{-1}), φ is the heat flow (mW), t is the time *versus* heat flow (s).

The CO$_2$ saturated sample was regenerated in the same procedure as described above before adsorption was carried out at 60 °C. Thus, the cyclic performance during five recycles was explored.

3. Results and discussion

3.1. Characterization

TGA weight loss curves of ZK loaded with various amounts of TEPA and PEI are shown in Fig. 2a, and the corresponding DTG curves are shown in Fig. 2b. All samples exhibited original weight losses below 120 °C due to liberation of moisture and CO$_2$. The further remarkable weight loss emerged in the range of 125–400 °C for samples of TEPA-loaded ZK, and 190–400 °C for samples of PEI-loaded ZK. ZK-TEPA-50 displayed an maximum weight loss rate at 217 °C while 303 °C for ZK-PEI-50, which can be associated with the decomposition of TEPA and PEI, respectively. With the increase of the amine loadings, the sharp weight loss peak shifted slightly towards the higher temperature for both TEPA-loaded and PEI-loaded samples. The introduction of more TEPA or PEI into the nanoporous support increased the particle size of the sample, resulting in the increase of decomposition temperature.[35] Besides, higher decomposition temperatures for PEI-loaded samples than TEPA-loaded samples indicated that the thermal stability was enhanced as the amine molecular weight increased. In this stage, the weight losses of about 45.3%, 57.53%, 67.42% and 72.99% were obtained for ZK-TEPA-50, ZK-TEPA-60, ZK-TEPA-70 and ZK-TEPA-80, respectively. The actual amine contents were very close to the theoretical values, indicating that TEPA was loaded well onto the support during the impregnation process. While ZK-PEI-50, ZK-PEI-60, ZK-PEI-70 and ZK-PEI-80 showed the smaller weight losses of about 39.23%, 51.25%, 63.49% and 76.71%, respectively. It can be ascribed to the larger amine molecular size and viscosity of PEI. PEI with large molecular size is not easy to enter the support and its large viscosity made the agglomeration occur more easily. As temperature exceeded 400 °C, there was no obvious weight loss and the different remaining weights were observed at 800 °C. It was due to the high heat resistant silica existing in the molecular sieve framework. ZK loaded with TEPA and PEI displayed thermal stability in N$_2$ up to 125 and 190 °C, respectively, which indicated that the regeneration temperature of 110 °C was suitable for the cyclic adsorption/desorption on all the samples.

The amount of amine groups impregnated in the ZK can also be determined by elemental analysis. Nitrogen contents in ZK modified with TEPA or PEI are listed in Table 1. When amine loading increased from 50 to 80%, the nitrogen contents increased from 12.06 to 20.46 mmol g^{-1} for TEPA-loaded samples, while 9.54 to 17.66 mmol g^{-1} for PEI-loaded samples, which were in close agreement with TGA results.
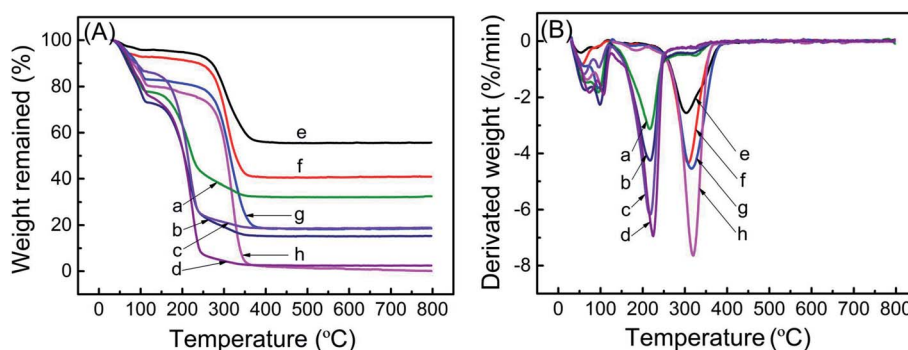

Fig. 2 (A) TGA curves and (B) DTG curves of (a) ZK-TEPA-50, (b) ZK-TEPA-60, (c) ZK-TEPA-70, (d) ZK-TEPA-80, (e) ZK-PEI-50, (f) ZK-PEI-60, (g) ZK-PEI-70 and (h) ZK-PEI-80.

Table 1 Textural properties, nitrogen contents, CO_2 adsorption capacities and amine efficiencies of amine modified ZK adsorbents at 60 °C
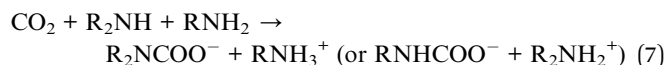
Adsorbent	S_{BET} (m^2 g^{-1})	V_{total} (cm^3 g^{-1})	Nitrogen content (mmol g^{-1})	Capacity (mmol g^{-1})	Amine efficiency (mmol CO_2/mmol N)
ZK-PEI-50	73.2	0.20	9.54	3.24	0.34
ZK-PEI-60	23.9	0.08	12.89	4.49	0.35
ZK-PEI-70	9.7	0.03	15.02	3.93	0.26
ZK-PEI-80	—	—	17.66	2.91	0.16
ZK-TEPA-50	94.3	0.25	12.06	4.27	0.35
ZK-TEPA-60	40.9	0.09	14.03	5.32	0.38
ZK-TEPA-70	30.8	0.07	16.19	4.85	0.30
ZK-TEPA-80	—	—	20.46	4.76	0.23

The FTIR spectra of ZK support, TEPA-loaded ZK and PEI-loaded ZK are shown in Fig. 3. The characteristic bands of KIT-6 around 1096, 802 and 459 cm^{-1} were identified over all the samples due to Si–O–Si asymmetric, symmetric stretching and bending vibrations, respectively.[36–38] While the band at 544 cm^{-1} associated with typical vibration modes of ZSM-5 (five-membered rings of T–O–T, T = Si or Al) in ZK shifted slightly towards the higher wavenumbers as shown in the spectra of ZK-TEPA-60 and ZK-PEI-60. The bands at 3467, 1638 and 967 cm^{-1} were associated with O–H stretching vibration of silanol groups, H–O–H bend, and Si–O stretching vibration of free silanol groups, respectively.[39,40] After TEPA or PEI impregnation, these bands either got weakened or eliminated entirely, which indicated that a part amount of amine groups in TEPA or PEI can interact with free silanol groups in ZK. The relevant reaction equations are given as follows:

$$Si–OH + RNH_2 \rightarrow Si–O^-N^+H_3R \quad (3)$$

$$Si–OH + R_2NH \rightarrow Si–O^-N^+H_2R_2 \quad (4)$$
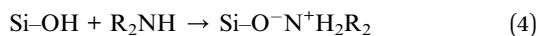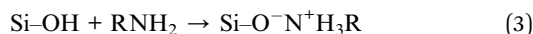
Besides the elimination of the band of free silanol groups, some new bands around 2956, 2854, 1634, 1573, 1481 and 1320 cm^{-1} appeared after TEPA or PEI loading in ZK. The bands around 2956 and 2854 cm^{-1} were associated with C–H asymmetric and symmetric stretching vibrations, while the band around 1481 cm^{-1} was associated with C–H deformation.[41,42] A weak band around 1634 cm^{-1} was found, related to N–H

deformation of protonated primary amine groups (Si–O–N$^+$H$_3$R) or secondary amine groups (Si–O–N$^+$H$_2$R$_2$) formed through reactions in eqn (3) and (4). The bands around 1573 and 1319 cm^{-1} were respectively associated with N–H deformation of primary amine groups and C–N stretching vibration.[42,43] The spectra of ZK-TEPA-60 and ZK-PEI-60 after CO_2 adsorption are also included in Fig. 3. A new band at 1415 cm^{-1} was identified in both spectra, attributed to NCOO skeletal vibration of carbamate formed from the reactions between amine groups and CO_2 molecules. These reactions that may occur during CO_2 adsorption process are depicted as follows:

$$CO_2 + 2RNH_2 \rightarrow RNHCOO^- + RNH_3^+ \quad (5)$$

$$CO_2 + 2R_1R_2NH \rightarrow R_1R_2NCOO^- + R_1R_2NH_2^+ \quad (6)$$

$$CO_2 + R_2NH + RNH_2 \rightarrow$$
$$R_2NCOO^- + RNH_3^+ \text{ (or } RNHCOO^- + R_2NH_2^+) \quad (7)$$

The N$_2$ adsorption/desorption isotherms of TEPA-loaded ZK and PEI-loaded ZK belonging to type IV isotherms are shown in Fig. 4, while the textural properties such as specific surface area (S_{BET}) and total pore volume (V_{total}) were listed in Table 1. When amine loading increased from 50 to 70%, the value of S_{BET} decreased from 73.2 to 9.7 m^2 g^{-1} for PEI-loaded samples, while 94.3 to 30.8 m^2 g^{-1} for TEPA-loaded samples. Similarly, the value of V_{total} decreased from 0.20 to 0.03 cm^3 g^{-1} for PEI-loaded samples, while 0.25 to 0.07 cm^3 g^{-1} for TEPA-loaded samples.

3.2. CO_2 adsorption

The CO_2 adsorption curves of ZK loaded with various amounts of TEPA and PEI with an adsorption temperature of 60 °C are shown in Fig. 5a and b, respectively. The adsorption data is given in Table 1. When amine loading was 50%, ZK-TEPA-50 demonstrated an appreciable adsorption capacity of 4.27 mmol g^{-1}, whereas ZK-PEI-50 demonstrated that of 3.24 mmol g^{-1}. The maximum values in the two series were 5.32 and 4.49 mmol g^{-1} for ZK-TEPA-60 and ZK-PEI-60, respectively. The increase of adsorption capacity was due to the increased nitrogen content and the enhanced chemisorption between amine groups and CO_2 (Table 1, Fig. 5). Despite the reduction of physisorption due to the decrease of surface area and pore volume, the enhanced chemisorption due to the increase of nitrogen content may be dominant in the CO_2 adsorption,
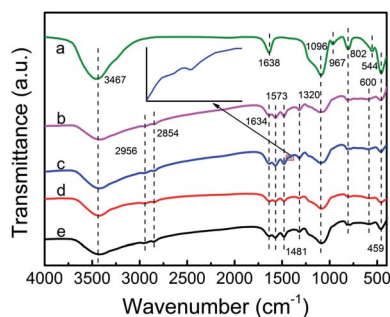
Fig. 3 FTIR spectra of (a) ZK, (b) ZK-TEPA-60, (c) ZK-TEPA-60 after CO_2 adsorption, (d) ZK-PEI-60 and (e) ZK-PEI-60 after CO_2 adsorption.
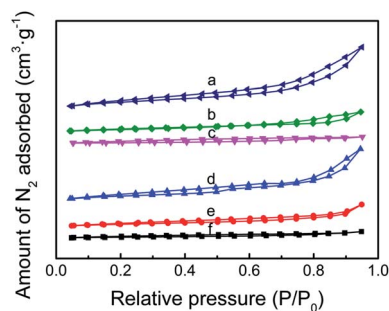
Fig. 4 (A) N_2 adsorption/desorption isotherms of (a) ZK–TEPA-50, (b) ZK–TEPA-60, (c) ZK–TEPA-70, (d) ZK–PEI-50, (e) ZK–PEI-60 and (f) ZK–PEI-70.

resulting in the increase of adsorption capacity (Table 1, Fig. 5). Increasing amine loading to 70%, the capacity decreased to 4.85 mmol g^{-1} for ZK-TEPA-70 and 3.93 mmol g^{-1} for ZK-PEI-70. Further increasing amine loading to 80%, the value decreased to 4.76 mmol g^{-1} for ZK-TEPA-80, but ZK-PEI-80 demonstrated an apparent decrease in uptake of 2.91 mmol g^{-1}. Mesoporous structure of KIT-6 in the composites offered large space and channel for the loading of amine groups as well as CO_2 diffusion and the microporous structure of ZSM-5 in the composites played a major role in physisorption of CO_2. Although the nitrogen contents in the two series increased significantly as amine loadings were increased to 70%, this property could not compensate for the great losses of surface area as well as pore volume (Table 1). The high loading of

amines blocked the ZSM-5 pores and limited the diffusion of CO_2 to ZSM-5 channels and to the active adsorption sites on amine groups, resulting in the lower adsorption capacities compared to the maximum values.

On the other hand, TEPA-loaded samples displayed higher CO_2 adsorption capacities compared to those of corresponding PEI-loaded samples. For ZK-TEPA-X, TEPA was well dispersed in the inner channels of composites even at high loading of 60% while retaining a pore volume of 0.09 cm^3 g^{-1} as well as a surface area of 40.9 m^2 g^{-1}, because of its low molecular weight and linear properties (Table 1). These common effects were beneficial to the improvement of adsorption capacity due to the easiness for CO_2 to overcome the diffusion resistance and access to the active sites. For ZK-PEI-X, due to the high molecular weight and polymeric properties of PEI, the dispersion of PEI in composites was low and the significant losses of pore volume and surface area were found (Table 1). These effects caused damage to the accessibility of PEI and resulted in the lower adsorption capacities compared to those of ZK-TEPA-X. It can be concluded that the amine content (nitrogen content) and the accessibility of active sites on amine groups to interact with CO_2 are the important factors for the efficient use of an adsorbent in CO_2 capture.

In addition, the amine efficiency of the adsorbents calculated from the ratio between CO_2 capture capacity and nitrogen content are given in Table 1. CO_2 adsorption capacity and amine efficiency with amine loading for ZK-TEPA-X and ZK-PEI-X are shown in Fig. 6a and b, respectively. The reaction between CO_2
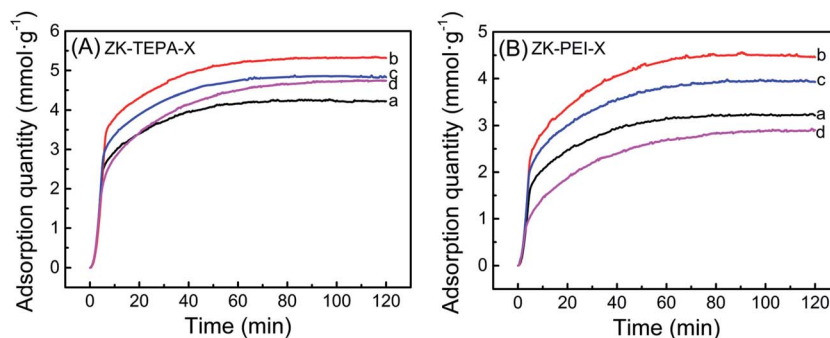

Fig. 5 (A) CO_2 adsorption curves of (a) ZK–TEPA-50, (b) ZK–TEPA-60, (c) ZK–TEPA-70 and (d) ZK–TEPA-80 and (B) CO_2 adsorption curves of (a) ZK–PEI-50, (b) ZK–PEI-60, (c) ZK–PEI-70 and (d) ZK–PEI-80 (adsorption at 60 °C, inlet CO_2 concentration: 15 vol%, gas flow rate: 60 cm^3 min^{-1}).
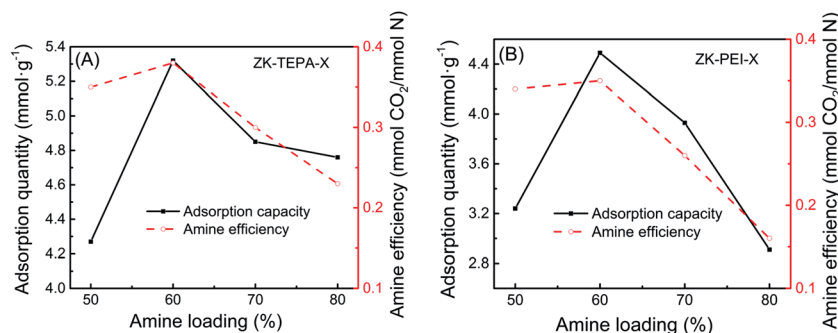

Fig. 6 CO_2 adsorption capacity and amine efficiency with amine loading for (A) ZK-TEPA-X and (B) ZK-PEI-X.

and amine groups needs two amine groups per CO_2 molecule (eqn (4)–(6)), so the amine efficiency should not exceed 0.5 normally.[44] The similar trends were observed in both series. The amine efficiency increased first and then decreased with the increase of amine loadings. ZK-TEPA-60 displayed an maximum amine efficiency of 0.38, which was higher than that of ZK-PEI-60 (0.35).

The adsorption temperature is an important factor for chemisorption of CO_2, so the effects of various temperatures (30, 45, 60, 75 and 90 °C) on adsorption capacities of ZK-TEPA-60 and ZK-PEI-60 were investigated as shown in Fig. 7a and b, respectively. For ZK-TEPA-60, the adsorption capacity increased in the temperature range of 30–60 °C while decreased in range of 60–90 °C. The similar trend was observed for ZK-PEI-60 while the optimum temperature of ZK-PEI-60 (75 °C) shifted towards a higher value compared to that of ZK-TEPA-60 (60 °C), which may be due to the different natures of TEPA and PEI molecules. The increase in adsorption capacity at the first temperature period indicated the dominant contribution of chemisorption for CO_2 adsorption capacity, which was based on two reasons. One reason is that the CO_2 molecule overcame the kinetic limitation and the faster diffusion of CO_2 molecule was achieved at higher temperatures. Another reason is that the TEPA and PEI molecules were more flexible and their dispersions were more uniform in the mesopores, and more active adsorption sites on amine groups were exposed to CO_2 molecules at higher temperatures.

The capacity decreased at the second temperature period. The adsorption progress was dependent on thermodynamics at relatively high temperatures. At this period, CO_2 molecules were activated with slightly higher kinetic energy and the part of them overcame the chemical bonds and van der Waals' force between the surface of ZK-TEPA-60 or ZK-PEI-60 and CO_2 molecules. The adsorption capacities of ZK-TEPA-60 at 30, 45, 60, 75 and 90 °C were, 4.44, 4.53, 5.32, 4.85 and 4.62 mmol g^{-1}, respectively, while 3.85, 3.95, 4.49, 4.59 and 4.43 mmol g^{-1} for ZK-PEI-60. Their adsorption capacities are all higher than 3 mmol g^{-1}, especially for ZK-TEPA-60, indicating that both ZK-TEPA-60 and ZK-PEI-60 are potentially efficient sorbents for CO_2 capture.

A comparison of CO_2 adsorption capacity *via* various amine modified adsorbents is given in Table 2. Under similar conditions, both ZK-TEPA-60 and ZK-PEI-60 obtained in this work displayed outstanding adsorption capacities at a low CO_2 partial pressure.

What's more, in the practical adsorption operation, the adsorption kinetics should be carefully taken into account. In this work, the adsorption time was selected to achieve 50 and 85% of the equilibrium adsorption capacities for the two best samples in the two series (ZK-TEPA-60 and ZK-PEI-60) at three temperatures as shown in Fig. 8 and Table 3. At 30 and 90 °C,
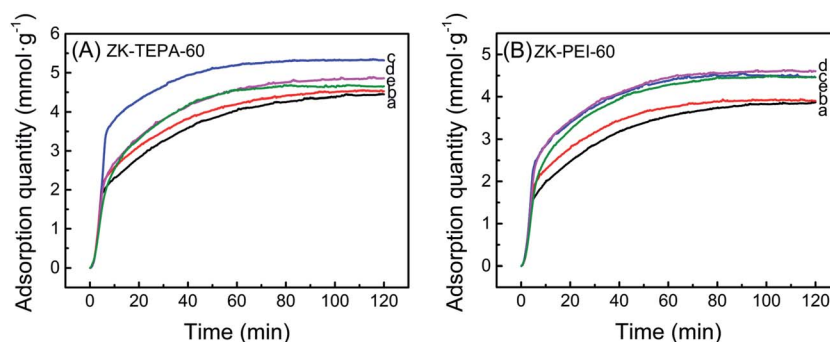

Fig. 7 CO_2 adsorption curves of (A) ZK-TEPA-60 and (B) ZK-PEI-60 at (a) 30 °C, (b) 45 °C, (c) 60 °C, (d) 75 °C and (e) 90 °C (inlet CO_2 concentration: 15 vol%, gas flow rate: 60 cm^3 min^{-1}).

Table 2 CO_2 adsorption capacities of various adsorbents from literatures and our work[a]

Support	Modifier	W_t (%)	Condition	Capacity (mmol g^{-1})	Method	Ref.
Y60	TEPA	50	60 °C/15 kPa	2.56	Grafting	45
SBA-16	AEAPS	15	60 °C/15 kPa	0.73	Grafting	46
ZSM-5	PEI	33.3	40 °C/101 kPa	2.64	Impregnation	47
ZSM-5	TEPA	50	25 °C/20 kPa	0.98	Impregnation	48
KIT-6	PEI	50	75 °C/101 kPa	3.07	Impregnation	22
KIT-6	TEPA	50	60 °C/10 kPa	2.85	Impregnation	49
5A@MSA	PEI	30	25 °C/15 kPa	1.63	Impregnation	31
ZSM-5/KIT-6	TEPA	60	60 °C/15 kPa	5.32	Impregnation	This work
ZSM-5/KIT-6	PEI	60	60 °C/15 kPa	4.49	Impregnation	This work

[a] W_t: weight percent of modifiders. Condition: pressure was the CO_2 partial pressure with dry condition. Y60: Y-type zeolite with a Si/Al molar ratio of 60. AEAPS: *N*-(2-aminoethyl)-3-aminopropyltrimethoxysilane. 5A@MSA: 5A@MSA was combined with 5A zeolite and mesoporous silica.
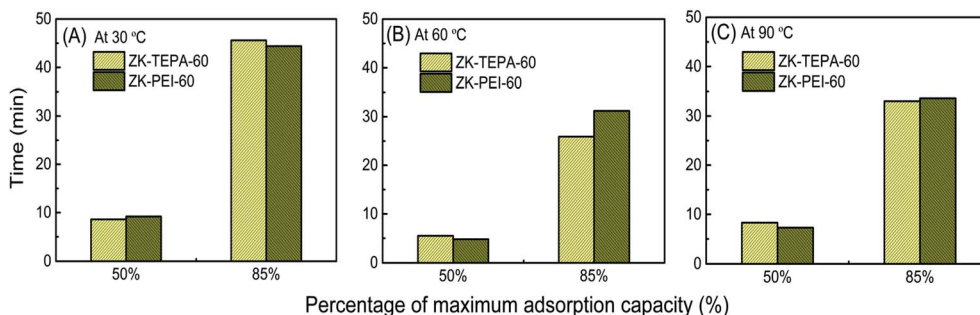
Fig. 8 Adsorption time of ZK–TEPA-60 and ZK–PEI-60 at (A) 30 °C, (B) 60 °C and (C) 90 °C using 15% CO_2.

Table 3 Adsorption kinetics and enthalpies of ZK–PEI-60 and ZK–TEPA-60 at three different temperatures

Adsorbent	Temperature (°C)	Time taken to reach a percentage of the maximum capacity (min)		Enthalpy (kJ mol⁻¹)	Average enthalpy (kJ mol⁻¹)
		50%	85%		
ZK-PEI-60	30	9.2	44.4	67.3	70
	60	4.8	31.2	71.9	
	90	7.3	33.6	70.9	
ZK-TEPA-60	30	8.6	45.6	71.2	75.2
	60	5.5	25.9	81.2	
	90	8.3	33	73.3	

both samples displayed small differences in time to achieve 50 and 85% of the maximum adsorption capacities, indicating the similar kinetics. At 30 and 90 °C, respectively, ZK-TEPA-60 required 45.6 and 33 minutes and ZK-PEI-60 required 44.4 and 33.6 minutes to achieve 85% of the maximum adsorption capacities (Table 3, Fig. 8). While at 60 °C, the differences in time to achieve 85% of the maximum adsorption capacities were obvious between both samples (25.9 minutes for ZK-TEPA-60 and 31.2 minutes for ZK-PEI-60) (Table 3, Fig. 8). Therefore, TEPA-loaded samples displayed better kinetics than PEI-loaded samples. Normally, more time is required to adsorb additional CO_2 to reach high adsorption capacity, while ZK-TEPA-60, which possesses higher CO_2 adsorption capacity, interestingly, has better kinetics. This result was due to the well dispersion of

TEPA molecules in the inner channels of composites for the easy diffusion of CO_2 molecules, suggesting the importance of uniform dispersion of amine molecules for enhanced kinetics.

The heat of adsorption, usually defined as the enthalpy (H_{ads}) of adsorption, was obtained by calorimetric heat flow measurement for further characterization of adsorption. The differential scanning calorimetry (DSC) heat flow curves of ZK-TEPA-60 and ZK-PEI-60 at three different temperatures are shown in Fig. 9. The enthalpies of adsorption are given in Table 3. The adsorption enthalpies of ZK-TEPA-60 at 30, 60 and 90 °C were, 71.2, 81.2 and 73.3 kJ mol⁻¹, respectively, while 67.3, 71.9 and 70.9 kJ mol⁻¹ for ZK-PEI-60. These values were all higher than 60 kJ mol⁻¹, which were consistent with the chemisorption mechanism, revealing the dominance of
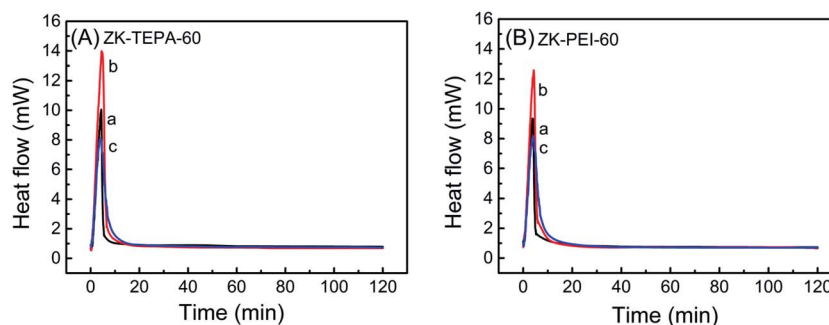

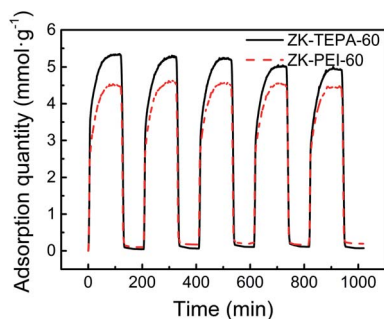Fig. 9 DSC heat flow curves of (A) ZK-TEPA-60 and (B) ZK-PEI-60 at (a) 30 °C, (b) 60 °C and (c) 90 °C using 15% CO_2.

Fig. 10 Cyclic adsorption/desorption runs of ZK–TEPA-60 and ZK–PEI-60 (adsorption at 60 °C, desorption at 110 °C, nitrogen flow rate: 100 cm^3 min^{-1}, gas flow rate: 60 cm^3 min^{-1}).

chemisorption during the CO_2 adsorption process.[50] These values correlated well with previously reported data.[51,52] The average enthalpy of 75.2 kJ mol^{-1} was obtained for ZK-TEPA-60 and 70 kJ mol^{-1} for ZK-PEI-60, both of which were slightly larger than the values obtained by Knowles *et al.* for aminopropyl-functionalized silica gel.[52] These differences can be associated with various natures of amines. For both samples, the trends on enthalpies are similar to those on adsorption capacities and the high enthalpies suggest the high strength of CO_2–amine interaction (Fig. 7).

Apart from high adsorption capacity, the stability and reproducibility of adsorbents are also essential for the sustainable application process. ZK-TEPA-60 and ZK-PEI-60 were selected for the five cyclic CO_2 adsorption/desorption studies. The graphs of five cycles for ZK-TEPA-60 and ZK-PEI-60 are shown in Fig. 10. After the five cycles, ZK-PEI-60 displayed a stable capacity of 4.45 mmol g^{-1}, which was similar to the initial one (4.49 mmol g^{-1}). However, a relatively large drop of 7% in adsorption capacity occurred for ZK-TEPA-60, compared to that of ZK-PEI-60 (less than 1%), which may be attributed to the partial volatilization of TEPA in desorption step. ZK-PEI-60 has a better stability and reproducibility than ZK-TEPA-60 during 5 cyclic adsorption/desorption process. But obviously, ZK-TEPA-60 still displayed a large capacity of 4.94 mmol g^{-1} in the 5th cycle, which is still higher than the reported data as listed in Table 2. The stability of ZK-TEPA-60 is comparable to that of TEPA modified MCM-41 (8.5% drop in adsorption capacity after 6 cycles) reported by Yue *et al.*[53] These results suggest that both ZK-TEPA-60 and ZK-PEI60 are good CO_2 adsorbents and the latter may be the more promising one. Besides, water vapor also exists in flue gas and the CO_2 uptake may be enhanced due to the existence of appropriate content of water vapor.[54,55] The effect of water vapor will be reported in the future.

4.   Conclusions

The ZSM-5/KIT-6 support was modified with amines (TEPA or PEI) by wet impregnation. The amine efficiency, kinetics of adsorption, enthalpy of adsorption, stability of adsorbent, reusability of adsorbent, the effect of TEPA or PEI loading as

well as temperature on CO_2 adsorption performance were investigated. ZK-TEPA-60 displayed the maximum adsorption capacity at 60 °C while a lower value for ZK-PEI-60 was obtained (5.32 mmol g^{-1} *vs.* 4.49 mmol g^{-1}) because of higher nitrogen content and better texture properties. The amine efficiency was up to 0.38 and 0.35 for ZK-TEPA-60 and ZK-PEI-60, respectively. The optimum temperature was 60 °C for ZK-TEPA-60 while 75 °C for ZK-PEI-60 (with a capacity of 4.59 mmol g^{-1}), probably associated with different natures of amine molecules. ZK-TEPA-60 has better kinetics than ZK-PEI-60 due to the well dispersion of TEPA molecules. Higher average enthalpy was obtained for ZK-TEPA-60 (75.2 kJ mol^{-1}) compared to that of ZK-PEI-60 (70 kJ mol^{-1}), suggesting the high strength of CO_2–amine interaction. ZK-PEI-60 has a better stability and reproducibility than ZK-TEPA-60 during five cyclic adsorption/desorption process.

Conflicts of interest

There are no conflicts of interest to declare.

Acknowledgements

References

1 S. Choi, J. H. Drese and C. W. Jones, *ChemSusChem*, 2009, **2**, 796–854.

2 D. W. Keith, *Science*, 2009, **325**, 1654.

3 M. G. Plaza, C. Pevida, B. Arias, M. D. Casal, C. F. Martín, J. Fermoso, F. Rubiera and J. J. Pis, *J. Environ. Eng.*, 2009, **135**, 426–432.

4 C. Pevida, M. G. Plaza, B. Arias, J. Fermoso, F. Rubiera and J. J. Pis, *Appl. Surf. Sci.*, 2008, **254**, 7165–7172.

5 B. Li, Y. Duan, D. Luebke and B. Morreale, *Appl. Energy*, 2013, **102**, 1439–1447.

6 W. Conway, S. Bruggink, Y. Beyad, W. Luo, I. Melián-Cabrera, G. Puxty and P. Feron, *Chem. Eng. Sci.*, 2015, **126**, 446–454.

7 F. J. Tamajón, E. Álvarez, F. Cerdeira and D. Gómez-Díaz, *Chem. Eng. J.*, 2016, **283**, 1069–1080.

8 M. G. Plaza, C. Pevida, A. Arenillas, F. Rubiera and J. J. Pis, *Fuel*, 2007, **86**, 2204–2212.

9 L. Wang, L. Ma, A. Wang, Q. Liu and T. Zhang, *Chin. J. Catal.*, 2007, **28**, 805–810.

10 M. G. Plaza, C. Pevida, B. Arias, J. Fermoso, A. Arenillas, F. Rubiera and J. J. Pis, *J. Therm. Anal. Calorim.*, 2008, **92**, 601–606.

11 G. D. Pirngruber, F. Guillou, A. Gomez and M. Clausse, *Int. J. Greenhouse Gas Control*, 2013, **14**, 74–83.

12 R. S. Pillai and E. Titus, *Materials Today: Proceedings*, 2015, **2**, 446–455.

13 S. Couck, J. Lefevere, S. Mullens, L. Protasova, V. Meynen, G. Desmet, G. V. Baron and J. F. M. Denayer, *Chem. Eng. J.*, 2017, **308**, 719–726.

14 Z. Zhang, H. Wang, X. Chen, R. Xie, P. Gao, W. Wei and Y. Sun, *Adsorption*, 2014, **20**, 883–888.

15 R. Kishor and A. K. Ghoshal, *RSC Adv.*, 2016, **6**, 898–909.

16 L. Du, Z. Lu, L. Xu and J. Zhang, *RSC Adv.*, 2017, **7**, 21268–21272.

17 Z. Qiao, J. Zhou and X. Lu, *Fluid Phase Equilib.*, 2014, **362**, 342–348.

18 Z. Qiao, N. Wang, J. Jiang and J. Zhou, *Chem. Commun.*, 2016, **52**, 974–977.

19 P. Ammendola, F. Raganati and R. Chirone, *Chem. Eng. J.*, 2017, **322**, 302–313.

20 J. Wei, Z. Lin, Z. He, L. Geng and L. Liao, *Water, Air, Soil Pollut.*, 2017, **228**, 128.

21 M. Hefti, D. Marx, L. Joss and M. Mazzotti, *Microporous Mesoporous Mater.*, 2015, **215**, 215–228.

22 W.-J. Son, J.-S. Choi and W.-S. Ahn, *Microporous Mesoporous Mater.*, 2008, **113**, 31–40.

23 S. C. G. Santos, S. W. M. Machado, A. M. Garrido Pedrosa and M. J. B. Souza, *J. Porous Mater.*, 2015, **22**, 1145–1151.

24 H. Nigar, B. Garcia-Baños, F. L. Peñaranda-Foix, J. M. Catalá-Civera, R. Mallada and J. Santamaría, *AIChE J.*, 2016, **62**, 547–555.

25 S. Loganathan and A. K. Ghoshal, *Chem. Eng. J.*, 2017, **308**, 827–839.

26 M. Niu, H. Yang, X. Zhang, Y. Wang and A. Tang, *ACS Appl. Mater. Interfaces*, 2016, **8**, 17312–17320.

27 A. Gholidoust, J. D. Atkinson and Z. Hashisho, *Energy Fuels*, 2017, **31**, 1756–1763.

28 Y. Zhao, Y. Shen, L. Bai, R. Hao and L. Dong, *Environ. Sci. Technol.*, 2012, **46**, 1789–1795.

29 Y. Zhao, Y. Shen, G. Ma and R. Hao, *Environ. Sci. Technol.*, 2014, **48**, 1601–1608.

30 R. Kishor and A. K. Ghoshal, *Chem. Eng. J.*, 2015, **262**, 882–890.

31 X. Liu, F. Gao, J. Xu, L. Zhou, H. Liu and J. Hu, *Microporous Mesoporous Mater.*, 2016, **222**, 113–119.

32 Y. Zhao, Y. Shen and L. Bai, *J. Colloid Interface Sci.*, 2012, **379**, 94–100.

33 C. He, J. Li, X. Zhang, L. Yin, J. Chen and S. Gao, *Chem. Eng. J.*, 2012, **180**, 46–56.

34 Z. Lin, J. Wei, L. Geng, D. Mei and L. Liao, *Water, Air, Soil Pollut.*, 2017, **228**, 412.

35 P. Zeng, S. Zajac, P. C. Clapp and J. A. Rifkin, *Mater. Sci. Eng., A*, 1998, **252**, 301–306.

36 D. Zhang, A. Duan, Z. Zhao and C. Xu, *J. Catal.*, 2010, **274**, 273–286.

37 W. Wang, J. Xiao, X. Wei, J. Ding, X. Wang and C. Song, *Appl. Energy*, 2014, **113**, 334–341.

38 W. Wang, X. Yang, Y. Fang and J. Ding, *Appl. Energy*, 2009, **86**, 170–174.

39 Y. Jiang, Q. Gao, H. Yu, Y. Chen and F. Deng, *Microporous Mesoporous Mater.*, 2007, **103**, 316–324.

40 V. Umamaheswari, M. Palanichamy and V. Murugesan, *J. Catal.*, 2002, **210**, 367–374.

41 M. R. Mello, D. Phanon, G. Q. Silveira, P. L. Llewellyn and C. M. Ronconi, *Microporous Mesoporous Mater.*, 2011, **143**, 174–179.

42 B. Singh and V. Polshettiwar, *J. Mater. Chem. A*, 2016, **4**, 7071.

43 A. C. C. Chang, S. S. C. Chuang, M. Gray and Y. Soong, *Energy Fuels*, 2003, **17**, 468–473.

44 R. Sanz, G. Calleja, A. Arencibia and E. S. Sanz-Pérez, *Microporous Mesoporous Mater.*, 2012, **158**, 309–317.

45 F. Su, C. Lu, S.-C. Kuo and W. Zeng, *Energy Fuels*, 2010, **24**, 1441–1448.

46 J. Wei, J. Shi, H. Pan, W. Zhao, Q. Ye and Y. Shi, *Microporous Mesoporous Mater.*, 2008, **116**, 394–399.

47 C. H. Lee, D. H. Hyeon, H. Jung, W. Chung, D. H. Jo, D. K. Shin and S. H. Kim, *J. Ind. Eng. Chem.*, 2015, **23**, 251–256.

48 L.-Y. Lin, J.-T. Kuo and H. Bai, *J. Hazard. Mater.*, 2011, **192**, 255–262.

49 Y. Liu, Q. Ye, M. Shen, J. Shi, J. Chen, H. Pan and Y. Shi, *Environ. Sci. Technol.*, 2011, **45**, 5710–5716.

50 D. Madden and T. Curtin, *Microporous Mesoporous Mater.*, 2016, **228**, 310–317.

51 C. Knöfel, J. Descarpentries, A. Benzaouia, V. Zeleňák, S. Mornet, P. L. Llewellyn and V. Hornebecq, *Microporous Mesoporous Mater.*, 2007, **99**, 79–85.

52 G. P. Knowles, J. V. Graham, S. W. Delaney and A. L. Chaffee, *Fuel Process. Technol.*, 2005, **86**, 1435–1448.

53 M. B. Yue, L. B. Sun, Y. Cao, Y. Wang, Z. J. Wang and J. H. Zhu, *Chem.–Eur. J.*, 2008, **14**, 3442–3451.

54 R. A. Khatri, S. S. C. Chuang, Y. Soong and M. Gray, *Ind. Eng. Chem. Res.*, 2005, **44**, 3702–3708.

55 X. Xu, C. Song, J. M. Andrésen, B. G. Miller and A. W. Scaroni, *Microporous Mesoporous Mater.*, 2003, **62**, 29–45.